Hindawi
International Journal of Energy Research
Volume 2024, Article ID 8851270, 12 pages
https://doi.org/10.1155/2024/8851270

Research Article

Studies toward Morphological Changes of Silver/Carbon Fiber Composites and Their Optimization for High-Performance Electrochemical Electrodes

Taehan Yeo, Kyungmin Kim, Jaeho Lee, Byungseok Seo, Seonghyun Park, and Wonjoon Choi

School of Mechanical Engineering, Korea University, Seoul, Republic of Korea 02841

Correspondence should be addressed to Wonjoon Choi; wojchoi@korea.ac.kr

Received 22 August 2023; Revised 20 March 2024; Accepted 22 March 2024; Published 17 April 2024

Academic Editor: Rami Reddy Boppella

The integration of micro/nanostructured metal/metal oxides with carbon-based materials has emerged as a promising approach for developing electrochemical electrodes. However, the fabrication of such hybrids entails complex and multistep procedures involving the grain boundaries and interfaces between the constituent materials, thus, degrading the overall performance. Herein, we report a facile electrothermal process (ETP) for the scalable fabrication of hybrid carbon fiber (CF) sheets integrated with tunable morphology of silver micro/nanoparticles. The application of an electric field across the layered film, consisting of $AgNO_3$ and CF, enabled the rapid dissipation of thermochemical energy in an open-air environment via ETP. The ETP facilitated ultrafast heat dissipation within a few milliseconds, leading to the rapid decomposition of $AgNO_3$, which resulted in the formation of liquefied Ag on the CF surface affording a reduced Ag-CF composite with adjustable structures through input power. The capability of ETP driven by controlling duration and number of electrical pulses was demonstrated by examining the corresponding physiochemical and electrochemical characteristics of the resulting composite. The Ag-CF composite fabricated using three cycles of a screened ETP pulse (1500 W and 75 ms for power and duration) acted as a supercapacitor electrode demonstrating excellent area capacitance (13 F/cm^2) and exceptional capacitance retention (98% after 10,000 cycles). Thus, the utilization of ETP can provide manufacturing strategies enabling scalable synthesis of functional hybrids in vacuum-free ambient environments within milliseconds. These hybrids possess unique interfaces and particle boundaries, exhibiting considerable potential for diverse electrochemical applications.

1. Introduction

Silver is a highly desirable material for electrochemical applications owing to its exceptional physiochemical properties. The enhanced electrical conductivity of silver facilitates efficient electron transfer, resulting in accelerated electrochemical reactions [1–4]. Moreover, silver exhibits remarkable corrosion resistance [5, 6]. These favorable characteristics have advanced the utilization of silver in various electrical applications, including supercapacitors and catalysts [7–10]. However, the performance of silver-based systems varies depending upon the specific method used for their synthesis and their integration with support materials. The synthesis of silver nanoparticles can be achieved using diverse strategies, which include chemical reduction in solution, electrochemical techniques, ultrasonic organic chemistry, photocatalytic reduction, microwave organic synthesis, radiation reduction, and biomass reduction [11–17]. The synthesized nanoparticles show various morphologies such as nanowires, nanoplates, nanoflowers, and nanocubes, depending upon the synthetic procedures utilized [18–21]. Among these morphologies, silver spheres have been extensively used for applications in sensing, medical, and photocatalytic fields owing to their structural stability and compatibility with support materials [21–23]. However, the anisotropic and nonspherical growth of silver poses challenges to the synthesis of silver spheres, requiring specialized equipment and incurring high costs. Therefore, the advancement of cost-effective synthetic

processes, capable of producing silver nanospheres and controlling their morphology, holds the potential to foster progress in the fabrication of electrochemical electrodes.

To meet the requirements of commercial applications, electrochemical electrodes should possess high reactivity and a stable integration between active and support materials [24, 25]. Thus, it is crucial to investigate the physiochemical properties of the active and support materials to enhance the overall performance of the electrode system [26, 27]. Notably, highly porous supporting substrates facilitate the diffusion of reaction substances to electrically active regions within the electrodes [28–30]. Recently, carbon-based materials (e.g., carbon nanotube (CNT), graphene, carbon fiber (CF), and carbon felt) have emerged as promising materials for supporting electrochemical electrode materials owing to their porous networks, high electronic conductivity, and robust mechanical stability [31]. The integration of carbon materials with the active material generates a network that can reduce energy loss during electron transfer to the active site of materials compared to those for other substrates [32]. Simultaneously, this network promotes the charge transport of the electrode from the electrolyte, further enhancing the overall performance of the system [33–36]. Consequently, these materials have been extensively utilized as electrode substrates for manufacturing electrochemical devices [37, 38]. Additionally, the desired surface characteristics of carbon-based materials could be achieved via heat treatment [39–41]. This enables concurrent synthesis, modification, and optimization of the active material, support substrate, and integrated compound. Consequently, carbon-based substrates could significantly reduce the entire process cost.

Electrothermal process (ETP), which has gained recent attention, could induce rapid increase of the processing temperature for target precursors, resulting in unique physicochemical characteristics of the metal/carbon composites [42–44]. The facile synthesis induced by rapid temperature changes effectively causes defects in metal crystals and carbon-based materials which could not be obtained by conventional slow heating-cooling processes and enables the highly functional composites in terms of electrochemical electrodes and catalysts [45–47]. So far, although the efficacy of the ETP for synthesizing various hybrid composites has been demonstrated, adjusting the processing parameters for desired composites, such as operating temperatures and heating-cooling durations, has not been explored enough to precisely control the resulting products. Thus, in-depth study for the ETP processing parameters and produced composites of metal-carbon-based materials would be beneficial to apply this rapid thermal processing technique to various energy storage and conversion applications.

In this paper, we report a facile electrothermal process (ETP) for the direct fabrication of binder-free silver sphere-embedded CF sheets for generating high-performance electrochemical electrodes (Figure 1). Silver spheres were synthesized using a tunable ETP that optimized the dimensions of the silver spheres and the defective CF structures. This process synthesizes a hybrid structure incorporating various materials using thermal energy induced by electrothermal heating. The hybrid structure comprises metal oxide precursors and nanomaterials integrated with conductive carbon-based materials (carbon nanotubes, graphene, graphite, glassy carbon, etc.). When the temperature induced by the electric field reaches the decomposition temperature of the metal oxide precursor, it decomposes into a metal oxide. Additionally, oxygen is removed via the supplied high-temperature energy, resulting in the reduction of the metal oxide, which shows a phase change into the liquid metal form. Subsequently, the supply of thermal energy is stopped, and spherical nanoparticles are generated during the cooling process. The synthesized metal spheres penetrate the surface of the carbon-based material at high temperatures and form the composite structure of the sphere-embedded carbon material. The particle size, shape, and degree of embedding in the hybrid structure manufactured using the ETP process can be fine-tuned by regulating the applied electrical energy. In this study, changes in the surface, mechanical, chemical, and electrical properties were analyzed with variations in applied energy. Furthermore, the electrodes could be optimized by adjusting the number of ETP pulses, guided by the observed experimental trends. The process is exceptionally rapid and allows the preparation of film-form composites in a single step within milliseconds, making it economical and advantageous for thin-film electrode applications. Additionally, this work will provide insight into designing rapid thermal synthesis of metal/carbon composites and electrodes without the use of binders.

2. Materials and Methods

2.1. Synthesis of Metal Nitrate/Polymer-Coated CF Sheets. A mixture of deionized water, ethanol, and acetic acid was prepared with a volumetric ratio of 1 : 1 : 3, followed by the addition of polyvinylpyrrolidone (PVP, Sigma-Aldrich) and mixing using a Vortex Genie 2 Mixer. Subsequently, 0.1 M $AgNO_3$ (Sigma-Aldrich) was dissolved in the solution, and the resulting mixture was stirred at 60°C for 24 h using a magnetic stirrer to ensure complete dissolution. The prepared precursor solution was applied onto a $4 \times 4\,cm^2$ CF sheet and coated as a thin film using a spin coater (1500 rpm, 60 s). The film was subsequently cut into a size of $1 \times 4\,cm^2$, and a titanium electrode was affixed to each side for facilitating the Joule heating thermal process under an applied electric field.

2.2. ETP to Synthesize Silver Nanospheres. Each precursor/CF sheet film was cut to $1 \times 4\,cm^2$ size and then attached to silver paste at both ends of a $1 \times 1\,cm^2$ titanium foil, which served as an electrode for ETP. The terminals of a DC power supply (50 A, 30 V, and 1500 W) were connected to both electrodes, and a voltage of 1500 W was applied. Consequently, a high temperature was induced between the CF sheets by the Joule heating at a current of approximately 50 A. The applied voltage was cut off when the temperature reached its highest point and was cooled under ambient air and room temperature conditions (approximately 25°C). During this process, the nitrate group present in silver nitrate disappeared as NO_2 at the decomposition temperature, whereas the hydrate evaporated as water vapor

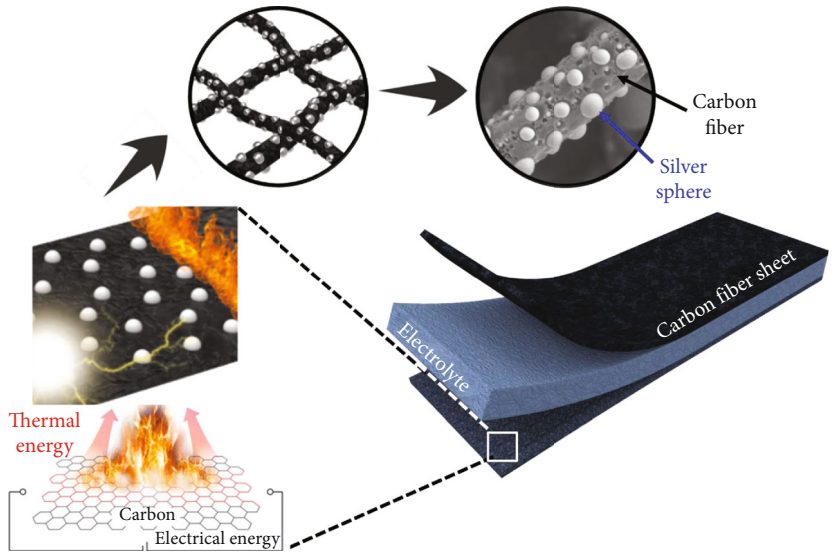

FIGURE 1: Schematic of the electrothermal process (ETP) for fabricating silver sphere-embedded CF (Ag-CF) sheets for high-performance electrochemical electrodes.

at a melting temperature of 100°C. When silver particles are melted, they merge with surrounding silver particles, thereby transforming into a unified single metal particle. During the process, sufficient heat to complete liquefaction of silver could induce the formation of a spherical structure due to surface tension. After the ETP process, the samples were cut to a size of $1 \times 2\,cm^2$ (approximately $1\,\Omega$) for the preparation of the electrodes to remove the regions, which were in contact with the titanium foil.

2.3. Physicochemical Characterization. Physiochemical characterization was carried out using scanning electron microscopy (SEM), field emission SEM (FEI, Model Quanta 250 FEG; Jeol, Model JSM-6701F), X-ray photoelectron spectroscopy (XPS; ULVAC-PHI, X-tool), and X-ray diffraction (XRD; Rigaku, SmartLab). The XRD patterns were acquired in 2θ mode with a scan speed of 2°/min.

2.4. Electrochemical Characterization of Supercapacitor Electrodes Using Hybrid Composites. A three-electrode electrochemical cell configuration was used to measure the electrochemical characteristics and performances. Cyclic voltammetry (CV) was conducted with scan rates of 5, 20, and 100 mV/s for electrochemical characterization. Electrochemical impedance spectroscopy (EIS) was also conducted with frequency range from 10^{-1} Hz to 10^5 Hz. Cyclic stability test was conducted with up to 1000 cycles of charge-discharge process based on CV method at scan rate of 100 mV/s. The working electrodes were hybrid composites of silver and CF sheets of $1 \times 1\,cm^2$, and the reference and counter electrodes were Hg/HgO and Pt wires, respectively. A potassium hydroxide (KOH, Sigma-Aldrich) aqueous solution (5 M) was used as the electrolyte. All the electrochemical measurements were conducted using a potentiostat (Gamry Instruments Interface 1000E).

3. Results and Discussion

A binder-free silver sphere-embedded CF sheet was directly fabricated using the ETP (Figure 1). Prolonged exposure to high temperature during ETP can damage the CF and lower the electronic conductivity and stability of electrodes [39]. However, the decomposition of the precursor to the intended active material is required. Therefore, we attempted to reduce the duration of ETP using 1500 W power, which thermally decomposes the silver nitrate within a few milliseconds. Figure 2 illustrates temperature changes during ETP using 1500 W power and the threshold of the chemical reaction. The time required for the entire process was a few milliseconds, thereby confirming that it is an exceptionally fast yet effective synthesis route for hybrid electrode materials. A structural comparison of the micro-nanostructures of the Ag-CF electrodes fabricated using ETP was carried out. The morphological transitions, nanostructures, and chemical crystal structures of the electrodes were analyzed using SEM and XRD at five different durations of the single electrical pulse process, i.e., 25, 50, 75, 100, and 125 ms pulses, as shown in Figures 3(a)–3(f). Figure 3(a) shows the SEM image of the Ag-CF produced by applying 1500 W power as a single 25 ms pulse to a CF sheet coated with silver nitrate. 30–300 nm-sized particles are formed on CFs with a thickness of approximately 5–7 μm. Particles within the size range of 30–100 nm exhibit a cube-shaped nanostructure, which is one of the typical crystal shapes of silver nitrate [48], whereas spherical and smooth-surfaced particles are observed for sizes larger than 100 nm. Moreover, the surface becomes smooth during the transformation as the solid surface instantaneously changes to liquid upon nitrate decomposition, and nanostructures form in a direction that minimizes the surface tension during rapid cooling. Silver reacts chemically, melts, and aggregates. The XRD pattern reveals the existence of

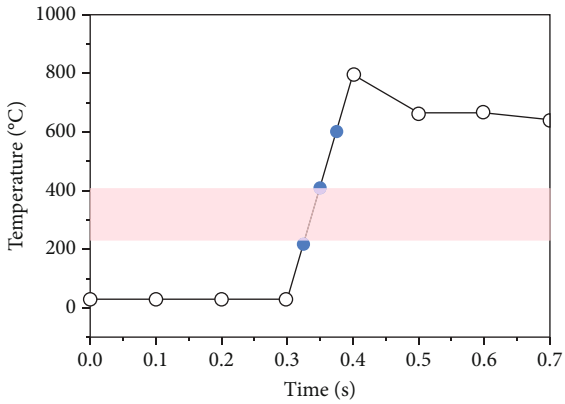

FIGURE 2: Real-time temperature profiles of precursor loaded CF sheet with 1500 W of the electrical pulse for 0.1 s duration. The light red regime indicates decomposition temperature of bulk silver nitrate. Blue dots represent the 25, 50, and 75 ms points, respectively. The temperature was measured by GL840 (GRAPHTEC) with k-type thermocouple.

both silver and silver nitrate (Figure 3(f)), which implies that the energy provided by a 25 ms pulse at 1500 W is insufficient for the complete conversion of silver nitrate into silver.

When the single pulse duration is increased to 50 ms (Figure 3(b)), the size of the particles obtained is 100–500 nm, which is larger than that in the case of single pulse with 25 ms. Additionally, all the particles change to silver, as given in Figure 3(f). Considering that silver is formed by the decomposition of silver nitrate, the size of the particles increases because the silver exists in a liquid state during the ETP process and longer duration increases the possibility to fuse with the surrounding particles. Therefore, silver nanostructures subjected to a 50 ms pulse aggregate randomly and spread over the CFs, resulting in a smooth surface.

Figure 3(c) shows the SEM image of the Ag-CF surface formed after applying a 75 ms pulse. Compared to the previous processes wherein energy was applied for a shorter period, the nanostructures of the Ag particles show a substantial change with the 75 ms pulse. Completely spherical Ag particles are formed on the surface of the CFs and embedded in the fibers rather than simply attaching to the surface. Additionally, the XRD pattern shows a similar intensity ratio to that of the JCPDS card (65–2871), which implies that it is stable silver. This result indicates that before the cooling process, the silver nitrate completely decomposes to form silver during the ETP process and combines with the surrounding particles in the liquid state, forming a single silver crystal particle during the cooling process. Furthermore, it has a spherical nanostructure that minimizes its surface energy. Figure S1 shows the change in grain size along the duration of the heating pulse. In contrast to the previously synthesized silver particles with random morphologies, these spherical particles offer the advantage of reduced electron movement loss during electrochemical reactions due to large grain size. Additionally, the spherical nanostructures exhibit enhanced resistance to failure by volume changes that occur during redox reactions due to the possibility of an isometric electrochemical reaction.

The surface morphology of the Ag/CF composite obtained by applying a 100 ms pulse is similar to that of the composite obtained by 75 ms pulse, wherein the Ag spheres are embedded in the CFs (Figure 3(d)). The size of the spheres is approximately 1–5 μm, and the diameter of the largest particle is similar to that of a CF. However, for the sample subjected to a 125 ms pulse, Ag particles are not observed on the CFs (Figure 3(e)) because the Ag particles decompose during the high-temperature ETP process, resulting in aggregation and separation from the fibers. Component analysis using the SEM images (Figures 3(a)–3(e)) revealed that the electrode manufactured by applying a power of 1500 W with 50, 75, and 100 ms pulses had the originally intended Ag-CF structure. Consequently, our investigation confirmed that the manipulation of crystal properties and the physical form of active materials can be achieved via a single-step procedure. Furthermore, we observed that the morphology of the support material utilized as a current collector could be controlled, enabling simultaneous control over the combined morphology. However, to achieve the desired application objectives, further optimization was required; therefore, the effect of the number of pulses on the physicochemical properties was investigated.

Figure 4 shows the morphological changes with different durations and the number of pulses applied. A trend between the morphological change of silver particles and CFs and applied heat energy could be identified. After the decomposition of silver nitrate, silver particles grow as observed with a single pulse at different durations. Comparing 50 ms and 75 ms, the particle growth rate seems to be affected by heat energy resulting in the melting and fusion of silver. If heat energy is not enough to melt the entire particle, the particle size exhibits a slow growth rate (Figures 4(a)–4(c)). Despite low heat energy provided by 50 ms pulse, silver penetrates and damages the CFs (Figure 4(c)) because silver promotes the complete oxidation of carbon [49]. Consequently, penetration occurs before the complete morphology change of silver particles. On the contrary, a fast growth rate is observed when the heat energy is enough to melt the entire particle (Figures 4(d) and 4(e)). Silver particles melt completely and assume a spherical shape owing to the heat provided by a 75 ms pulse. Thus, fusion takes place in a facile manner and triggers growth. Additionally, CFs show more damage by the larger silver particles. Finally, excessive heat (100 ms) damages both the silver particles and CFs. As depicted in Figure 3(e), it is observed that the silver detachment was initialized from the third pulse (Figure 4(h)). Consequently, CFs are destroyed, and a marginal quantity of silver particles was obtained after applying the pulse 5 times.

For investigating the electrochemical effects of morphological change, cyclic voltammetry was performed (Figure 5). An electrochemical test was performed on the supercapacitor by fabricating an electrode to compare the performance of the various Ag-CF films obtained by applying the ETP at various pulses. The experiment was conducted using a 3-electrode measurement method and an Ag-CF film. Silver was used as the active material for pseudo capacitance, and

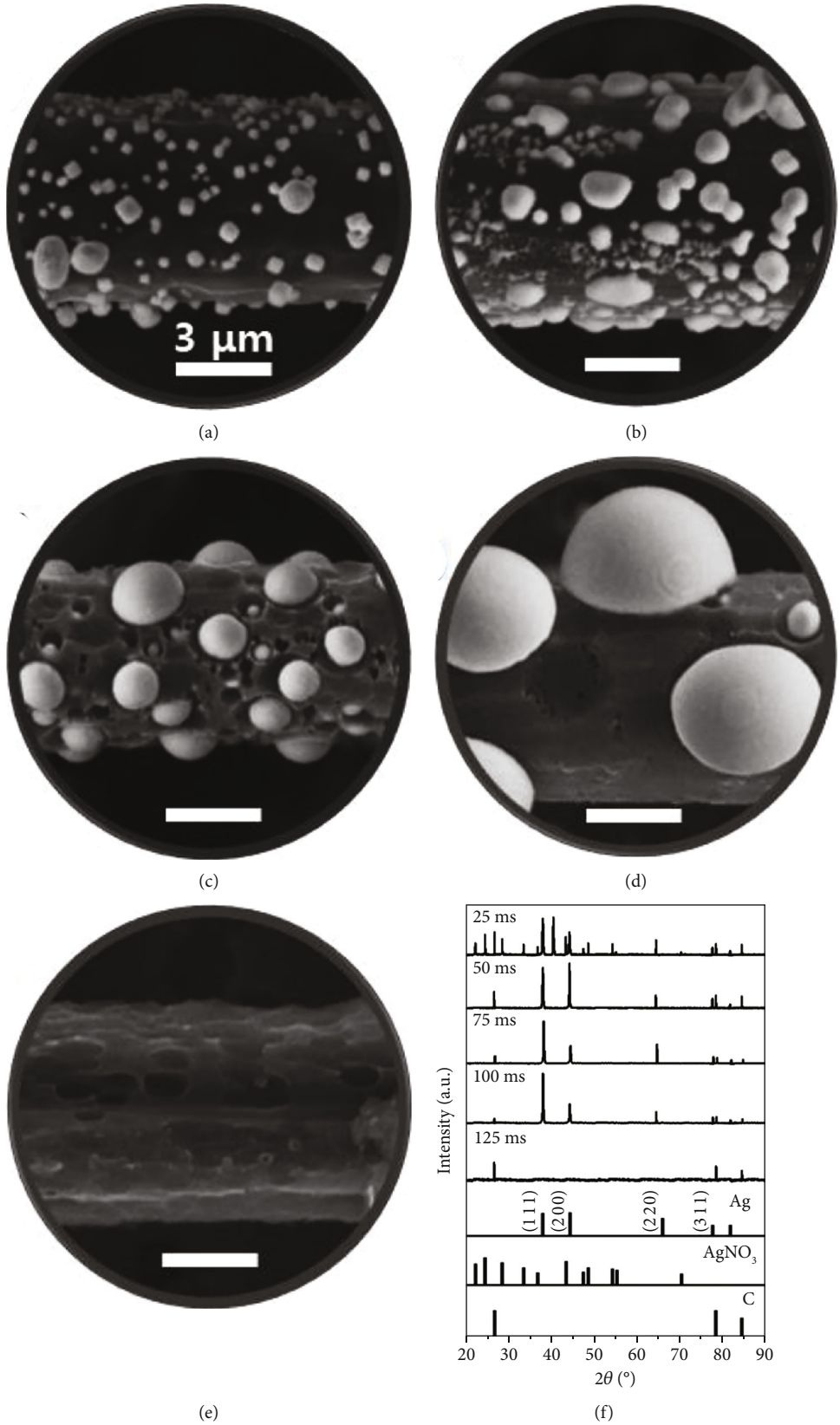

Figure 3: Physicochemical characterization of synthesized silver sphere-carbon sheets obtained with different duration of the ETP process. SEM images with single pulse durations of (a) 25, (b) 50, (c) 75, (d) 100, and (e) 125 ms at 30 V and 50 A (1500 W). (f) XRD patterns for each condition.

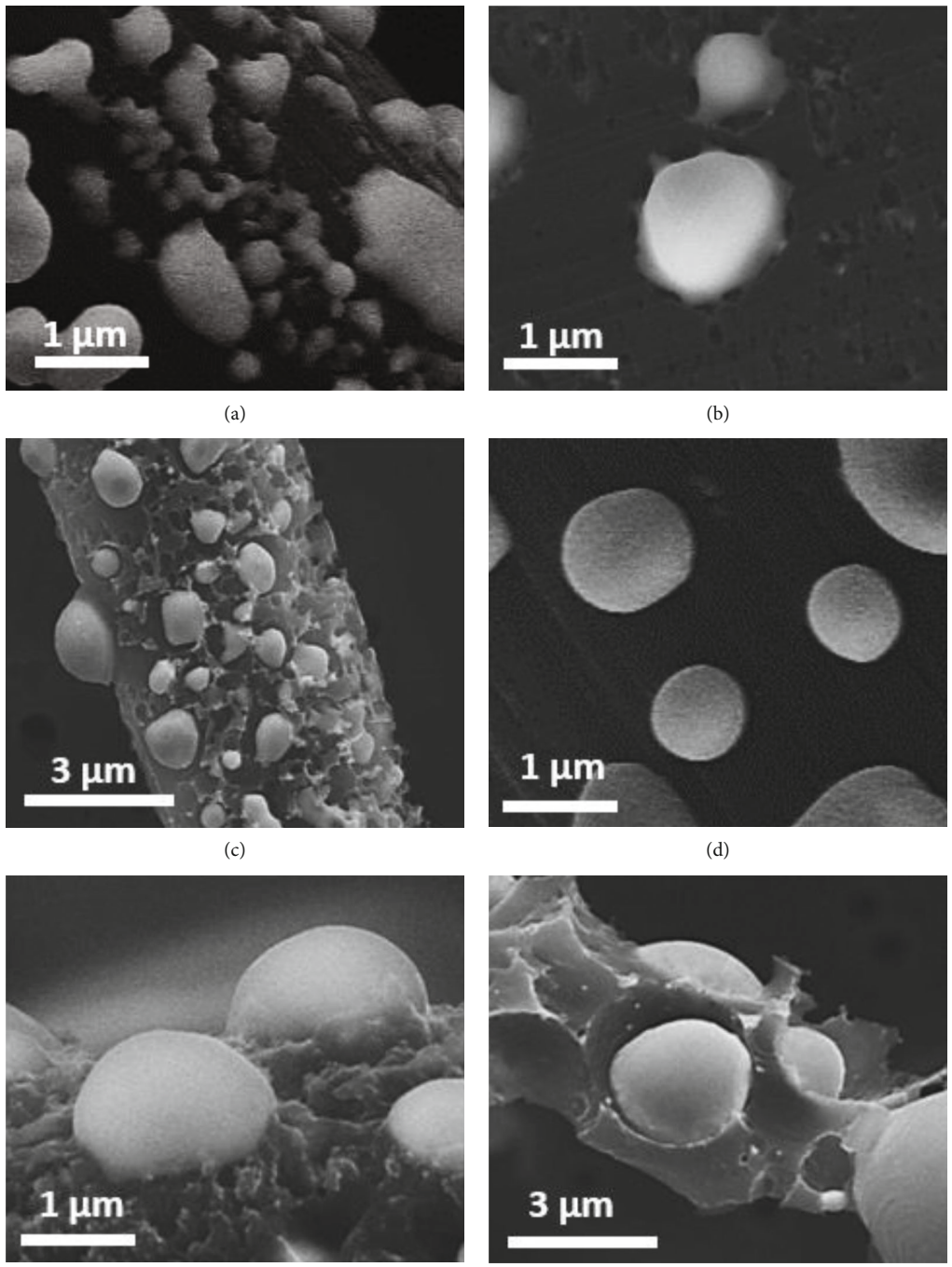

(a) (b) (c) (d) (e) (f)

Figure 4: Continued.

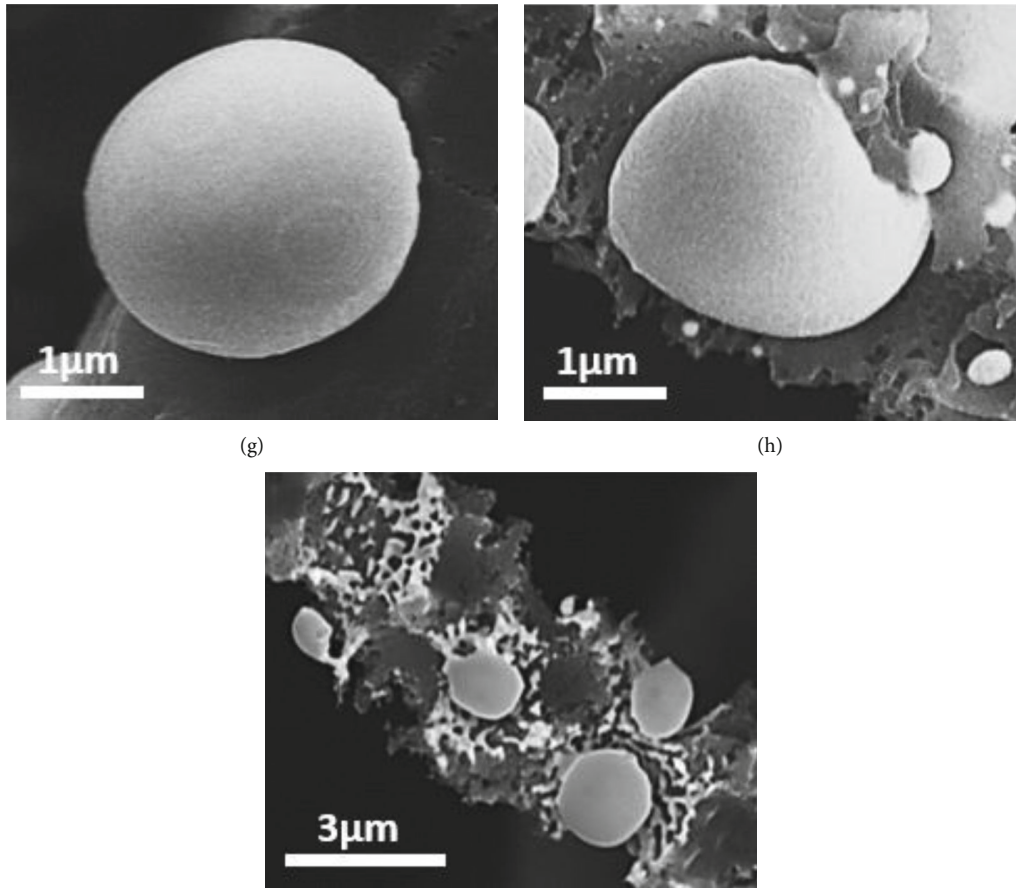

Figure 4: Morphological changes of silver sphere/carbon sheet synthesized using different conditions of the ETP process. SEM images of silver/carbon fiber synthesized using 1, 3, and 5 ETP pulses at (a–c) 50 ms, (d–f) 75 ms, and (g–i) 100 ms durations. Fixed power at 1500 W was applied for all processes.

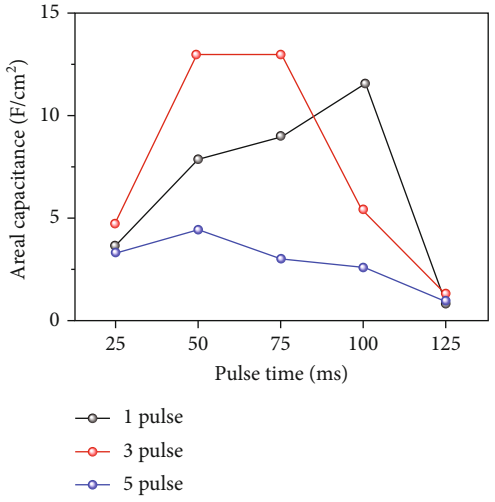

Figure 5: Comparison of areal capacitances of electrochemical electrodes comprising Ag-CF hybrid composites, according to changes in duration and number of ETP pulses.

CFs were used as the current collector for electrical double-layer capacitance (EDLC). KOH (5 M) was used as the electrolyte, and Hg/HgO was used as the reference electrode. A Pt wire was used as the counter electrode. Figure 5 illustrates the comparison of areal capacitance for Ag-CF films produced using various pulse durations in the ETP within a voltage window of -0.4–0.8 V at a scan rate of 5 mV/s. The Ag-CF samples produced with 1500 W power reveal an increase in areal capacitance with 100 ms pulse compared to that with 25 ms pulse and decrease substantially to that with 125 ms pulse. In the case of 25 ms pulse, the marginal contribution of silver to the capacitance is observed. As shown in Figure 3(f), it influences the incomplete transformation of silver nitrate whereas decreased capacitance of 125 ms pulse could be attributed to the separation of Ag particles from the CFs during the high-temperature process as evident by Figure 3(e).

In the case of the Ag-CF sample produced by applying three pulses of 1500 W power, the capacitance significantly increases for the electrodes obtained with 50 and 75 ms pulses (~13 F/cm^2) compared to that with the 25 ms pulse as they have embedded silver particles in the CFs. We confirmed the existence of silver at the highest capacitance condition using the XPS spectrum (Figure S2). As reported in

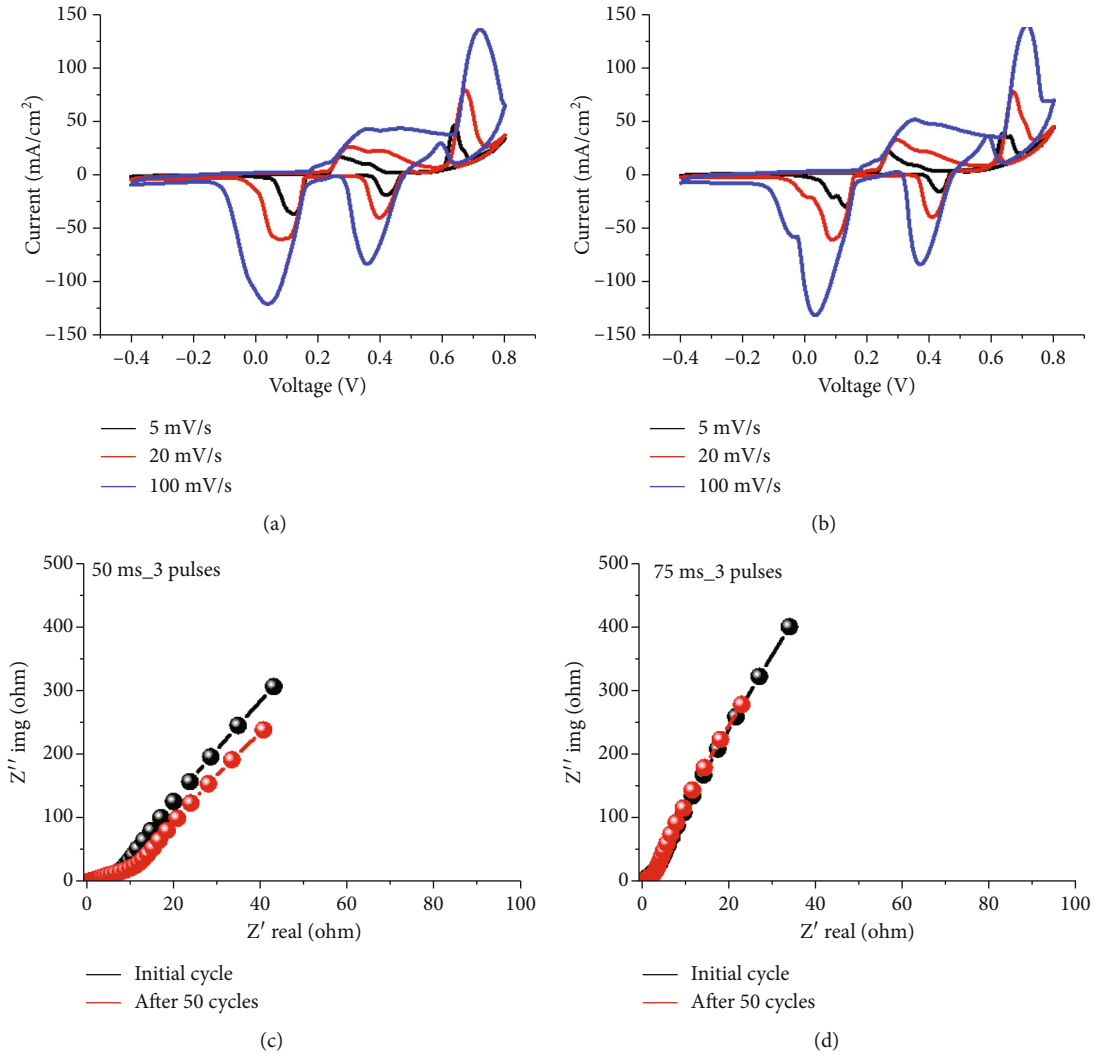

Figure 6: Electrochemical comparison of synthesized Ag-CF electrodes having the highest areal capacitance. Cyclic voltammetry (CV) curves of Ag-CF electrodes fabricated by 3 pulses of ETP with a duration of (a) 50 and (b) 75 ms. Nyquist plots of Ag-CF electrodes fabricated by 3 pulses of ETP with a duration of (c) 50 and (d) 75 ms.

our previous work [50], an increased contact area of active materials and current collector could reduce the resistance by the enlarged path of electrons. Furthermore, it could activate more silver particles to participate in the redox reaction. This is confirmed by comparing the CV curves obtained using 1 and 3 times of pulse applied (Figure S3), wherein 3 times of pulse show a more vigorous redox reaction despite a similar shape to that obtained using a pulse for a single time. In the case of the sample produced by applying a 100 ms pulse three times, the capacitance decreases significantly, which is in contrast to that produced by using 50 and 75 ms pulses because the Ag particles excessively penetrate the CFs destroying the fibers. Similarly, in the case of Ag-CFs manufactured by applying five pulses, CFs show a considerable number of defects in all the cases, and the capacitance is highly degraded because the destroyed CFs reduce conductivity [39].

Among all the ETP conditions, the highest areal capacitance is observed for the electrodes when the pulse was applied 3 times, with durations of 50 and 75 ms. Figure 6 shows the cyclic voltammograms (CV) and Nyquist plots of the electrode fabricated by applying 50 and 75 ms pulses 3 times. The scan rates for CV are selected to show the electrochemical characteristics considering areal performances [51–53]. The shape of the curves for supercapacitors with silver particles as the active material differs from that of EDLC because silver undergoes a redox reaction during the charge-discharge process, and two pairs of redox peaks are observed in the CV curves (Figures 6(a) and 6(b)). Each redox peak pair has positive and negative sweeps, and the phase change of silver and silver oxide during the redox reaction is given by the following equations [54]:

$$2\mathrm{Ag} + 2\mathrm{OH}- < - > \mathrm{Ag(I)_2O} + \mathrm{H_2O} + 2\mathrm{e}- \quad (1)$$

$$2\mathrm{Ag_2O} + 4\mathrm{OH}- < - > 4\mathrm{Ag(II)O} + 2\mathrm{H_2O} + 4\mathrm{e}- \quad (2)$$

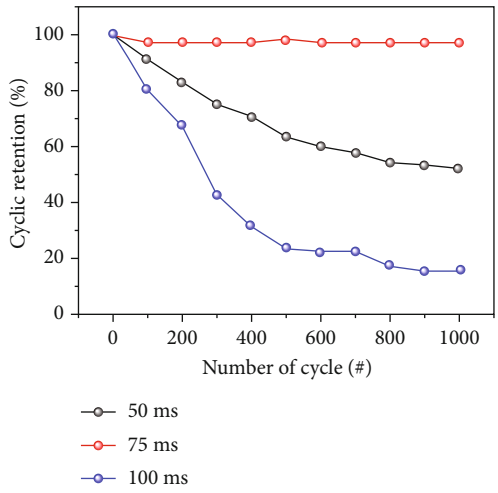

Figure 7: Cyclic stability of Ag-CF electrodes fabricated by 3 pulses of ETP with a duration of 50, 75, and 100 ms at a scan rate of 100 mV/s.

The areas of the CV curves are similar for the two types of electrodes obtained with 50 and 75 ms pulses, which implies that the initial areal capacitance values of the two electrodes are approximately the same. However, the Nyquist plots before and after charging and discharging the electrode 50 times at a scan rate of 100 mV/s exhibit different patterns. For the electrode manufactured by applying a 50 ms pulse three times, the slope of the graph decreases after 50 cycles, indicating that the electrode performance decreases during charging and discharging (Figure 6(c)), whereas for the Ag-CF electrode manufactured by applying a 75 ms pulse three times, the slope of the graph does not change even after 50 cycles of charging and discharging (Figure 6(d)). This difference could be attributed to the distinct structure of the synthesized Ag particles. The SEM images demonstrate that the Ag particle has an unspecified shape in the case of the 50 ms pulse (Figure 4(b)), whereas it is spherical in the case of 75 ms pulse (Figure 4(e)). As described in the redox reactions, the active material employing Ag undergoes oxidation and reduction via direct bonding with oxygen. It stores and releases electrons, resulting in repetitive volume changes. When a volume change occurs on the surface, in the case of a perfect sphere, the configuration is relatively stable owing to less change of surface area and structural properties [55, 56]. However, for particles with an unspecified shape, the direction of the volume increase is inconsistent under repetitive volume changes, causing the active material to escape, thereby decreasing the performance.

Figure 7 presents the cyclic retention graph, which reveals the stability of the fabricated electrode over 1000 charging and discharging cycles. Electrodes obtained by applying three different pulses show changes in the capacitance during 1000 charging and discharging cycles. In the case of 50 ms pulse process, after 1000 cycles, the retention is 60% because silver particles that did not have a completely spherical shape separate from the CFs because of the volume change occurring in the redox reaction. However, in the case of 75 ms pulse process, silver particles form a fully developed spherical shape, maintaining a capacitance during the charging and discharging processes. The presence of singular spherical particles, which exhibit the same crystal plane in the radial direction, minimizes the surface energy and confers strong mechanical properties against volume changes [57]. In the case of a 100 ms pulse, the capacitance decreases to 18% of the initial value after 1000 cycles owing to CF destruction by Ag particles. The comparative performances of supercapacitors using Ag-carbon-based hybrid materials as active materials are summarized in Table S1. The developed spherical Ag-CF electrode with 75 ms pulse process exhibits outstanding electrochemical performances in terms of areal capacitances and retention, compared with the different morphologies and carbon hybrids.

4. Conclusion

This study demonstrated the efficacy of pulsed ETP as an adjustable manufacturing process for Ag-CF in an open-air environment (25°C approximately) by optimizing the heating time and number of applied electrical pulses. The developed Ag-CF showed excellent electrochemical performance in terms of the capacitance ratio and cycle stability; hence, it was directly used as a flexible supercapacitor electrode. Silver nitrate and carbon sheet layered film, manufactured via spin coating, were employed in the ETP under various pulse conditions at 1500 W to produce Ag-CF. Complete reduction of $AgNO_3$ to Ag occurred during the nitrate decomposition in a high-temperature environment using the ETP. Moreover, unique structural characteristics were observed depending on the applied voltage and the number of pulses. The Ag-CF supercapacitor electrode fabricated by applying 75 ms pulses three times at 1500 W showed excellent areal capacitance (13 F/cm^2) and long-term capacitance retention over 10,000 charge/discharge cycles (98%). The Ag spheres embedded in the CF surface promoted charge transport in the active material, enhanced the conductivity of the electrode, and provided a stable interface for the redox reaction. In contrast, when Ag particles were not adequately embedded or were too large to damage the CFs, they showed low areal capacitance over 10,000 charge/discharge cycles and lower stability. The developed ETP can solve the scalability issue of metal/metal oxide/carbon-based materials, providing a facile and novel method for efficiently manipulating structural transformations, chemical compositions, and grain boundaries via the reduction process. The optimized ETP, which entails a millisecond-scale processing time, enables the structural synthesis of metals/metal oxides and complete bonding with a network of carbon-based materials via a one-step method. These versatile hybrids show excellent potential as supercapacitor electrodes with considerably enhanced performance and manufacturing scalability. We believe that the outcomes of this study will contribute to developing more scalable and versatile ETP fabrication techniques for not only supercapacitors but also a wide range of electrochemical electrodes for secondary batteries and catalysts, as well as electromagnetic interference shielding composites. Additionally, ETP could be performed at a minimal cost and high speed because it does not require

long processing times, voluminous installations, or special environments, making it an efficient method for the large-scale synthesis of micro/nanostructures.

Data Availability

The data that support the findings of this study are available from the corresponding author upon reasonable request.

Conflicts of Interest

The authors declare that they have no known competing financial interests or personal relationships that could have influenced the work reported in this study.

Authors' Contributions

Taehan Yeo and Kyungmin Kim contributed equally to this study.

Acknowledgments

This work was supported by the National Research Foundation of Korea (NRF) grant funded by the Korea government (Ministry of Science and ICT) (No. 2023R1A2C2006407 and No. 2020R1A5A1018153).

Supplementary Materials

Supplementary materials include supporting figures of variation of the average grain size of Ag particles (Figure S1), X-ray photoelectron spectroscopy (XPS) spectra of Ag-CF hybrid composites (Figure S2), cyclic voltammetry curves of Ag-CF electrodes obtained by applying different numbers of pulses with 50 and 75 ms duration (Figure S3), and an additional explanation about the calculation method of specific areal capacitances. *(Supplementary Materials)*

References

[1] N. Li, B. Huang, X. Dong et al., "Bifunctional zeolites-silver catalyst enabled tandem oxidation of formaldehyde at low temperatures," *Nature Communications*, vol. 13, no. 1, p. 2209, 2022.

[2] L. Wang, N. Kang, L. Gong et al., "A novel core-shell structured hybrid composed of zinc homobenzotrizoate and silver borotungstate with supercapacitor and photocatalytic dye degradation performance," *Journal of Energy Storage*, vol. 46, article 103873, 2022.

[3] Y. Chen, Y. Zhu, H. Sheng et al., "Molecular coadsorption of p-hydroxythiophenol on silver nanoparticles boosts the plasmon-mediated decarboxylation reaction," *ACS Catalysis*, vol. 12, no. 5, pp. 2938–2946, 2022.

[4] Z. Dai, P. G. Ren, Z. Guo et al., "Silver nanoparticles as a conductive bridge for high-performance flexible all-solid-state asymmetric supercapacitor," *International Journal of Energy Research*, vol. 46, no. 2, pp. 1813–1825, 2022.

[5] Y. Liu, X. Xu, Y. Wei et al., "Tailoring silver nanowire nanocomposite interfaces to achieve superior stretchability, durability, and stability in transparent conductors," *Nano Letters*, vol. 22, no. 9, pp. 3784–3792, 2022.

[6] Z. Zhao, J. Ma, M. Li, W. Liu, X. Wu, and S. Liu, "Model Ag/CeO_2 catalysts for soot combustion: roles of silver species and catalyst stability," *Chemical Engineering Journal*, vol. 430, article 132802, 2022.

[7] H. Ha, C. Amicucci, P. Matteini, and B. Hwang, "Mini review of synthesis strategies of silver nanowires and their applications," *Colloid and Interface Science Communications*, vol. 50, article 100663, 2022.

[8] A. Jain, M. Michalska, A. Zaszczyńska, and P. Denis, "Surface modification of activated carbon with silver nanoparticles for electrochemical double layer capacitors," *Journal of Energy Storage*, vol. 54, article 105367, 2022.

[9] R. A. Nuamah, S. Noormohammed, and D. K. Sarkar, "Supercapacitor performance evaluation of nanostructured Ag-decorated Co-Co_3O_4 composite thin film electrode material," *International Journal of Energy Research*, vol. 46, no. 9, pp. 13099–13110, 2022.

[10] A. Atta, M. M. Abdelhamied, D. Essam, M. Shaban, A. H. Alshammari, and M. Rabia, "Structural and physical properties of polyaniline/silver oxide/silver nanocomposite electrode for supercapacitor applications," *International Journal of Energy Research*, vol. 46, no. 5, pp. 6702–6710, 2022.

[11] F. E. Ettadili, M. Azriouil, B. Chhaibi et al., "Green synthesis of silver nanoparticles using Phoenix dactylifera seed extract and their electrochemical activity in Ornidazole reduction," *Food Chemistry Advances*, vol. 2, article 100146, 2023.

[12] X. Sun, Q. Qiang, Z. Yin, Z. Wang, Y. Ma, and C. Zhao, "Monodispersed silver-palladium nanoparticles for ethanol oxidation reaction achieved by controllable electrochemical synthesis from ionic liquid microemulsions," *Journal of Colloid and Interface Science*, vol. 557, pp. 450–457, 2019.

[13] W. B. Ayinde, W. M. Gitari, and A. Samie, "Optimization of microwave-assisted synthesis of silver nanoparticle by Citrus paradisi peel and its application against pathogenic water strain," *Green Chemistry Letters and Reviews*, vol. 12, no. 3, pp. 225–234, 2019.

[14] A. Massironi, A. Morelli, L. Grassi et al., "Ulvan as novel reducing and stabilizing agent from renewable algal biomass: application to green synthesis of silver nanoparticles," *Carbohydrate Polymers*, vol. 203, pp. 310–321, 2019.

[15] C. V. Restrepo and C. C. Villa, "Synthesis of silver nanoparticles, influence of capping agents, and dependence on size and shape: a review," *Environmental Nanotechnology, Monitoring & Management*, vol. 15, article 100428, 2021.

[16] N. Hashim, M. Paramasivam, J. S. Tan et al., "Green mode synthesis of silver nanoparticles using Vitis vinifera's tannin and screening its antimicrobial activity / apoptotic potential versus cancer cells," *Materials Today Communications*, vol. 25, article 101511, 2020.

[17] H. u. Hassan, M. W. Iqbal, A. M. Afzal et al., "Highly stable binary composite of nickel silver sulfide ($NiAg_2S$) synthesized using the hydrothermal approach for high-performance supercapattery applications," *International Journal of Energy Research*, vol. 46, no. 8, pp. 11346–11358, 2022.

[18] R. Gheitaran, A. Afkhami, and T. Madrakian, "Effect of light at different wavelengths on polyol synthesis of silver nanocubes," *Scientific Reports*, vol. 12, no. 1, article 19202, 2022.

[19] Y.-C. Lai, Y.-C. Wang, Y.-C. Chiu, and Y.-C. Liao, "Microwave-assisted synthesis for silver nanoplates with a high aspect ratio," *Langmuir*, vol. 37, no. 46, pp. 13689–13695, 2021.

[20] P. Zhang, I. Wyman, J. Hu et al., "Silver nanowires: synthesis technologies, growth mechanism and multifunctional applications," *Materials Science and Engineering: B*, vol. 223, pp. 1–23, 2017.

[21] X. Lin, S. Lin, Y. Liu et al., "Facile synthesis of monodisperse silver nanospheres in aqueous solution via seed-mediated growth coupled with oxidative etching," *Langmuir*, vol. 34, no. 21, pp. 6077–6084, 2018.

[22] G. Liao, Q. Li, W. Zhao, Q. Pang, H. Gao, and Z. Xu, "In-situ construction of novel silver nanoparticle decorated polymeric spheres as highly active and stable catalysts for reduction of methylene blue dye," *Applied Catalysis A: General*, vol. 549, pp. 102–111, 2018.

[23] F. Naaz, U. Farooq, M. A. M. Khan, and T. Ahmad, "Multifunctional efficacy of environmentally benign silver nanospheres for organic transformation, photocatalysis, and water remediation," *ACS Omega*, vol. 5, no. 40, pp. 26063–26076, 2020.

[24] M. Akin and X. Zhou, "Recent advances in solid-state supercapacitors: from emerging materials to advanced applications," *International Journal of Energy Research*, vol. 46, no. 8, pp. 10389–10452, 2022.

[25] M. Ali, A. M. Afzal, M. W. Iqbal et al., "2D-TMDs based electrode material for supercapacitor applications," *International Journal of Energy Research*, vol. 46, no. 15, pp. 22336–22364, 2022.

[26] S. A. Ansari, N. Parveen, M. A. S. al-Othoum, and M. O. Ansari, "Effect of washing on the electrochemical performance of a three-dimensional current collector for energy storage applications," *Nanomaterials*, vol. 11, no. 6, p. 1596, 2021.

[27] M. Z. Ansari, K. M. Seo, S. H. Kim, and S. A. Ansari, "Critical aspects of various techniques for synthesizing metal oxides and fabricating their composite-based supercapacitor electrodes: a review," *Nanomaterials*, vol. 12, no. 11, p. 1873, 2022.

[28] L. Zhou, K. Zhang, Z. Hu et al., "Recent developments on and prospects for electrode materials with hierarchical structures for lithium-ion batteries," *Advanced Energy Materials*, vol. 8, no. 6, article 1701415, 2018.

[29] R. Nivetha, S. Sharma, J. Jana, J. S. Chung, W. M. Choi, and S. H. Hur, "Recent advances and new challenges: two-dimensional metal–organic framework and their composites/derivatives for electrochemical energy conversion and storage," *International Journal of Energy Research*, vol. 2023, Article ID 8711034, 47 pages, 2023.

[30] K.-H. Lo, K. S. Anuratha, C. C. Cheng et al., "In situ synthesis of ZIF-67 thin films using low temperature chemical vapor deposition to fabricate all-solid-state flexible interdigital in-planar microsupercapacitors," *International Journal of Energy Research*, vol. 2023, Article ID 3754111, 14 pages, 2023.

[31] H. I. Alrayzan, S. A. Ansari, and N. Parveen, "Fabrication of asymmetric supercapacitor device based on nickel hydroxide electrode-graphene assembly," *Journal of Nanoelectronics and Optoelectronics*, vol. 17, no. 3, pp. 536–543, 2022.

[32] Y. Wang, L. Zhang, H. Hou et al., "Recent progress in carbon-based materials for supercapacitor electrodes: a review," *Journal of Materials Science*, vol. 56, no. 1, pp. 173–200, 2021.

[33] J. Shi, B. Jiang, C. Li et al., "Review of transition metal nitrides and transition metal nitrides/carbon nanocomposites for supercapacitor electrodes," *Materials Chemistry and Physics*, vol. 245, article 122533, 2020.

[34] Q. Hong and H. Lu, "*In-situ* electrodeposition of highly active silver catalyst on carbon fiber papers as binder free cathodes for aluminum-air battery," *Scientific Reports*, vol. 7, no. 1, p. 3378, 2017.

[35] S. Kumar, G. Saeed, L. Zhu, K. N. Hui, N. H. Kim, and J. H. Lee, "0D to 3D carbon-based networks combined with pseudocapacitive electrode material for high energy density supercapacitor: a review," *Chemical Engineering Journal*, vol. 403, article 126352, 2021.

[36] P. Veerakumar, A. Sangili, S. Manavalan, P. Thanasekaran, and K.-C. Lin, "Research progress on porous carbon supported metal/metal oxide nanomaterials for supercapacitor electrode applications," *Industrial & Engineering Chemistry Research*, vol. 59, no. 14, pp. 6347–6374, 2020.

[37] A. Borenstein, O. Hanna, R. Attias, S. Luski, T. Brousse, and D. Aurbach, "Carbon-based composite materials for supercapacitor electrodes: a review," *Journal of Materials Chemistry A*, vol. 5, no. 25, pp. 12653–12672, 2017.

[38] V. V. N. Obreja, "On the performance of supercapacitors with electrodes based on carbon nanotubes and carbon activated material—a review," *Physica E: Low-dimensional Systems and Nanostructures*, vol. 40, no. 7, pp. 2596–2605, 2008.

[39] K. Kim, B. Seo, S. Park, D. Shin, S. Kim, and W. Choi, "Electrothermally driven nucleation energy control of defective carbon and nickel–cobalt oxide-based electrodes," *ACS Nano*, vol. 16, no. 6, pp. 9772–9784, 2022.

[40] H. Kwon, J. H. Lee, Y. Roh et al., "An electron-deficient carbon current collector for anode-free Li-metal batteries," *Nature Communications*, vol. 12, no. 1, article 5537, 2021.

[41] S. H. S. Pai, A. Sasmal, A. K. Nayak, and H. S. Han, "Facile solvothermal synthesis of NiO/g-C_3N_4 nanocomposite for enhanced supercapacitor application," *International Journal of Energy Research*, vol. 2023, Article ID 1524859, 18 pages, 2023.

[42] Y. Yao, Z. Huang, P. Xie et al., "Carbothermal shock synthesis of high-entropy-alloy nanoparticles," *Science*, vol. 359, no. 6383, pp. 1489–1494, 2018.

[43] B. Seo, W. Kim, S. Park, C. Song, S. Kim, and W. Choi, "Electrothermally tunable morphological and redox design of heterogeneous Pd/PdxOy/carbon for humidity-hydron-driven energy harvesters," *Nano Energy*, vol. 95, article 107053, 2022.

[44] W. Kim, D. Shin, B. Seo, S. Chae, E. Jo, and W. Choi, "Precisely tunable synthesis of binder-free cobalt oxide-based Li-ion battery anode using scalable electrothermal waves," *ACS Nano*, vol. 16, no. 10, pp. 17313–17325, 2022.

[45] Q. Dong, M. Hong, J. Gao et al., "Rapid synthesis of High-Entropy oxide microparticles," *Small*, vol. 18, no. 11, article 2104761, 2022.

[46] S. Park, B. Seo, D. Shin, K. Kim, and W. Choi, "Sodium-chloride-assisted synthesis of nitrogen-doped porous carbon shells via one-step combustion waves for supercapacitor electrodes," *Chemical Engineering Journal*, vol. 433, article 134486, 2022.

[47] S. Park, B. Seo, D. Shin et al., "Synthesis of carbon nanotube-iron oxide composites via combustion waves for hybrid Li-ion battery anodes," *Chemical Engineering Journal*, vol. 470, article 144260, 2023.

[48] S. H. Park, J. G. Son, T. G. Lee, H. M. Park, and J. o. Song, "One-step large-scale synthesis of micrometer-sized silver nanosheets by a template-free electrochemical method," *Nanoscale Research Letters*, vol. 8, no. 1, p. 248, 2013.

[49] S. Dey and G. C. Dhal, "Applications of silver nanocatalysts for low-temperature oxidation of carbon monoxide," *Inorganic Chemistry Communications*, vol. 110, article 107614, 2019.

[50] T. Yeo, B. Seo, J. Lee, S. Park, K. Kim, and W. Choi, "Ultrafast extreme thermal–electrical fabrication of volcano-shape-like core-shell Ag-MnxOy branches anchored on carbon as high-performance electrochemical electrodes," *Nano Energy*, vol. 91, article 106663, 2022.

[51] L. Wang, H. Yao, F. Chi et al., "Spatial-interleaving graphene supercapacitor with high area energy density and mechanical flexibility," *ACS Nano*, vol. 16, no. 8, pp. 12813–12821, 2022.

[52] R. Chen, H. Tang, P. He et al., "Interface engineering of biomass-derived carbon used as ultrahigh-energy-density and practical mass-loading supercapacitor electrodes," *Advanced Functional Materials*, vol. 33, no. 8, article 2212078, 2023.

[53] Q. Yang, Z. Li, and B. Xu, "Layered double hydroxide with interlayer quantum dots and laminate defects for high-performance supercapacitor," *Advanced Functional Materials*, vol. 33, no. 24, article 2300149, 2023.

[54] H. Luo, X. Ji, and S. Cheng, "Investigation into the electrochemical behaviour of silver in alkaline solution and the influence of Au-decoration using operando Raman spectroscopy," *RSC Advances*, vol. 10, no. 14, pp. 8453–8459, 2020.

[55] D. Wang, C. Zhou, B. Cao et al., "One-step synthesis of spherical Si/C composites with onion-like buffer structure as high-performance anodes for lithium-ion batteries," *Energy Storage Materials*, vol. 24, pp. 312–318, 2020.

[56] W. Sun, Y. Zhang, and F. Yang, "Tuning electrochemical performance of carbon-sphere-based supercapacitors by compressive stress," *Electrochimica Acta*, vol. 357, article 136874, 2020.

[57] T. Yeo, J. Lee, D. Shin, S. Park, H. Hwang, and W. Choi, "One-step fabrication of silver nanosphere-wetted carbon nanotube electrodes via electric-field-driven combustion waves for high-performance flexible supercapacitors," *Journal of Materials Chemistry A*, vol. 7, no. 15, pp. 9004–9018, 2019.